Report

Cell Reports

AgRP Neurons Regulate Bone Mass

Graphical Abstract

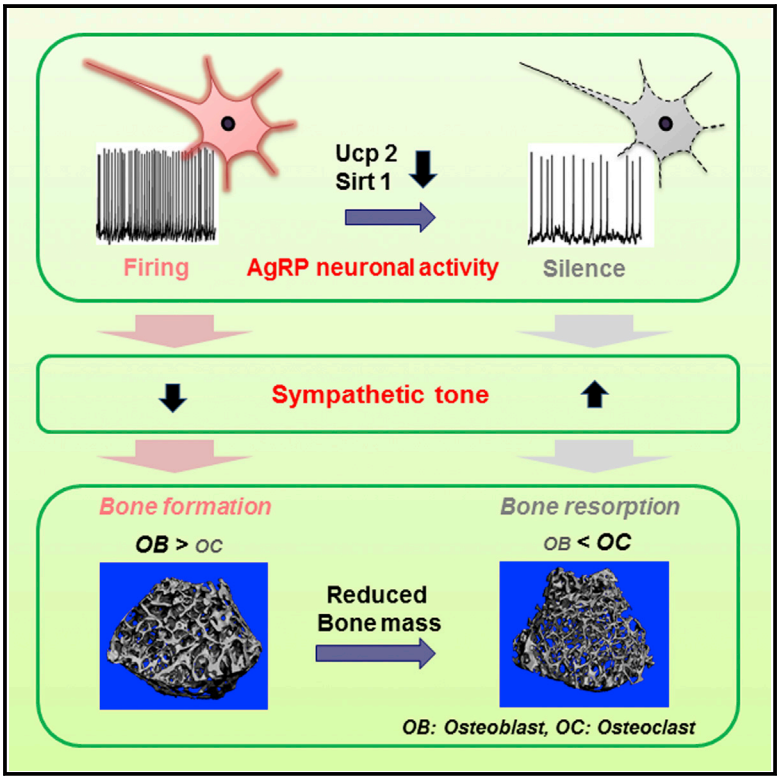

Authors

Jae Geun Kim, Ben-Hua Sun, Marcelo O. Dietrich, ..., Sabrina Diano, Karl Insogna, Tamas L. Horvath

Correspondence

tamas.horvath@yale.edu

In Brief

Kim et al. find that the AgRP neuronal circuit influences bone metabolism. Impaired AgRP circuit function leads to an osteopenic phenotype, suggesting that the effect of AgRP neurons on bone metabolism is mediated, at least in part, by the sympathetic nervous system.

Highlights

- Impaired AgRP neurons cause bone loss
- Enhanced AgRP neuronal activity increases bone mass
- Leptin receptors in AgRP neurons do not affect bone mass

Kim et al., 2015, Cell Reports *13*, 8–14
October 6, 2015 ©2015 The Authors
http://dx.doi.org/10.1016/j.celrep.2015.08.070

OPEN ACCESS
CellPress

Cell Reports
Report

AgRP Neurons Regulate Bone Mass

Jae Geun Kim,[1,3] Ben-Hua Sun,[2] Marcelo O. Dietrich,[1,4] Marco Koch,[1,5] Gang-Qing Yao,[2] Sabrina Diano,[1] Karl Insogna,[2,6] and Tamas L. Horvath[1,6,*]

[1]Program in Integrative Cell Signaling and Neurobiology of Metabolism, Section of Comparative Medicine
[2]Department of Internal Medicine
Yale University School of Medicine, New Haven, CT 06520, USA
[3]Division of Life Sciences, College of Life Sciences and Bioengineering, Incheon National University, Incheon 406-772, Republic of Korea
[4]Department of Biochemistry, Universidade Federal do Rio Grande do Sul, Porto Alegre RS 90035, Brazil
[5]Institute of Anatomy, University of Leipzig, 04103 Leipzig, Germany
[6]Co-senior author
*Correspondence: tamas.horvath@yale.edu
http://dx.doi.org/10.1016/j.celrep.2015.08.070

SUMMARY

The hypothalamus has been implicated in skeletal metabolism. Whether hunger-promoting neurons of the arcuate nucleus impact the bone is not known. We generated multiple lines of mice to affect AgRP neuronal circuit integrity. We found that mice with *Ucp2* gene deletion, in which AgRP neuronal function was impaired, were osteopenic. This phenotype was rescued by cell-selective reactivation of *Ucp2* in AgRP neurons. When the AgRP circuitry was impaired by early postnatal deletion of AgRP neurons or by cell autonomous deletion of *Sirt1* (AgRP-*Sirt1*$^{-/-}$), mice also developed reduced bone mass. No impact of leptin receptor deletion in AgRP neurons was found on bone homeostasis. Suppression of sympathetic tone in AgRP-*Sirt1*$^{-/-}$ mice reversed osteopenia in transgenic animals. Taken together, these observations establish a significant regulatory role for AgRP neurons in skeletal bone metabolism independent of leptin action.

INTRODUCTION

The skeleton provides physical support and protection of soft organ, houses the hematopoietic system, and allows for locomotion in support of survival. In vertebrates, bone is the principal reservoir of calcium, which is essential for cellular metabolism in all tissues. Thus, it is not surprising that evidence has emerged linking skeletal metabolism and whole body metabolic needs.

The central nervous system, and more specifically, the hypothalamus has a major regulatory role in peripheral tissue functions in health and disease (Dietrich et al., 2012; Matarese et al., 2013; Ruan et al., 2014; Warne et al., 2013). A growing body of evidence indicates that the hypothalamus also affects bone homeostasis mediated, at least in part, by the autonomic nervous system and endocrine organs (Ohlsson et al., 2012; Sato et al., 2007; Yadav et al., 2009). Hypothalamic neurons expressing agouti-related peptide (AgRP) drive hunger and have also been implicated in controlling peripheral tissues (Joly-Amado et al., 2012; Matarese et al., 2013), but to date have not been directly tied to the regulation of bone homeostasis. Using different lines of transgenic mice with altered AgRP neuronal function, the present study was undertaken to determine whether the AgRP circuit influences skeletal metabolism.

RESULTS

Ucp2 Impacts Bone Mass

Uncoupling protein 2 (Ucp2) is expressed in AgRP neurons (Coppola et al., 2007; Horvath et al., 1999), and AgRP neuronal activity is impaired in mice with global deletion of the *Ucp2* (Andrews et al., 2008). Structural analysis by microcomputed tomography (micro-CT) showed that 3-month-old male *Ucp2*$^{-/-}$ mice exhibited significantly reduced trabecular bone volume (BV/TV; Figure 1B) and trabecular thickness (Figure 1C). To clarify the cellular basis for these changes, histomorphometric analysis of trabecular bone from *Ucp2*$^{-/-}$ mice was performed and demonstrated a reduction in osteoblast number with no change in osteoclast number (Figure 1D), suggesting that Ucp2-regulated AgRP neuronal activity might affect bone remodeling processes by regulation of osteoblast formation and/or function. Since *Ucp2* is widely expressed (Diano and Horvath, 2012), and hence the bone phenotype of UCP2$^{-/-}$ mice might be the consequence of multiple mechanisms, we next generated mice (in collaboration with the Yale Genome Editing Center) in which *Ucp2* is selectively overexpressed in AgRP neurons (*Agrp-Ucp2*^{Tg} mice) using cre-lox technology (Figure S1A). We confirmed successful cre-mediated recombination in AgRP neurons by detecting EGFP positive cells in the hypothalamic arcuate nucleus (ARC) (Figure S1B). Bone mineral density (BMD) was significantly increased in 3-month-old male *Agrp-Ucp2*^{Tg} mice when analyzed by DXA (Figure 1E). To further test whether the osteopenia seen in global *Ucp2*-deficient mice could be due to altered AgRP neuronal activity, we crossed *Ucp*$^{-/-}$ mice with *Agrp-Ucp2*^{Tg} mice to generate mice with specific reactivation of *Ucp2* in AgRP neurons (*Ucp2*$^{-/-}$*:Agrp-Ucp2*^{Tg} mice). Micro-CT analysis revealed that the reduction in trabecular bone volume (Figure 1G) and thickness (Figure 1H) seen in global *Ucp2*-deficient mice was absent in 3-month-old male mice

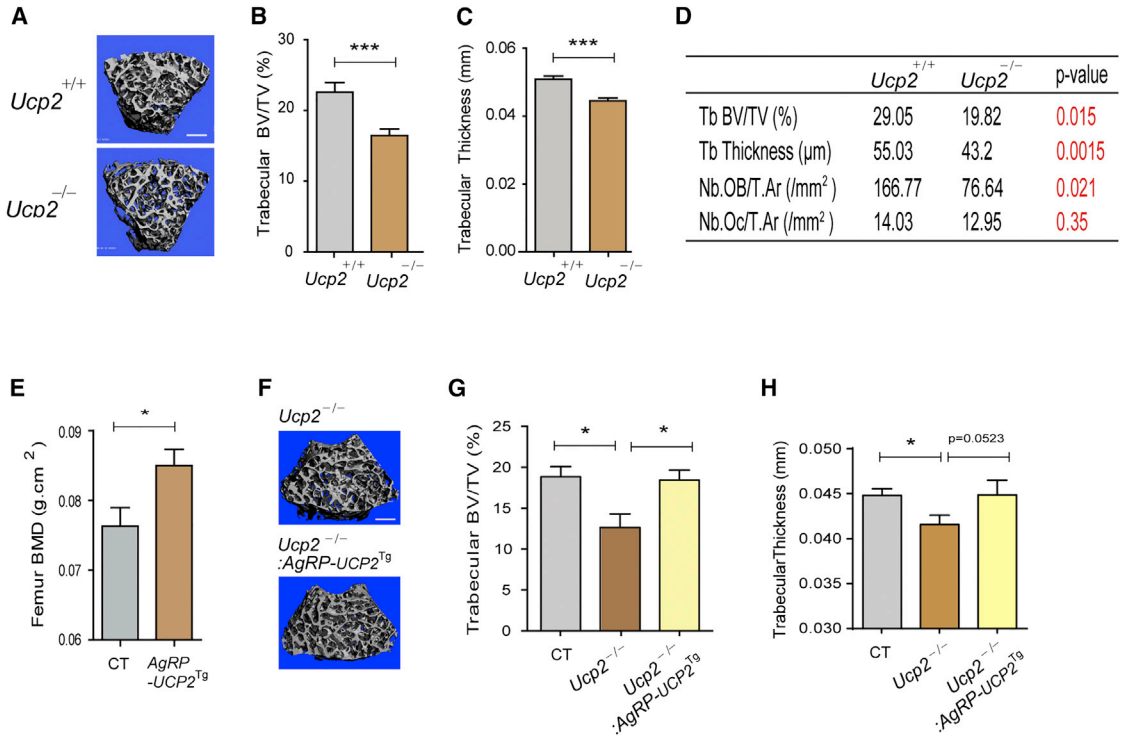

Figure 1. Altering AgRP Neuronal Activity by Deletion or Overexpression of *Ucp2* Affects Bone Mass

(A) Representative micro-CT images of femoral trabecular bone from 3-month-old male $Ucp^{+/+}$ and $Ucp^{-/-}$ mice. Scale bar, 500 μm.

(B and C) 3-month-old male $Ucp2^{-/-}$ mice exhibited reduced (B) trabecular bone volume (BV/TV) and (C) trabecular thickness (B: n = 10 for $Ucp2^{+/+}$, n = 12 for $Ucp2^{-/-}$, $p < 0.001$; C: n = 10 for $Ucp2^{+/+}$, n = 12 for $Ucp2^{-/-}$, $p < 0.001$).

(D) Histomorphometric analysis of trabecular bone from 3-month-old male $Ucp2^{-/-}$ mice revealed a reduced bone mass with a reduction in trabecular thickness and osteoblast number (n = 5 for $Ucp2^{+/+}$, n = 6 for $Ucp2^{-/-}$).

(E) DXA analysis demonstrated an increase in femoral BMD in 3-month-old male $Agrp\text{-}Ucp2^{Tg}$ mice (n = 6 for CT, n = 9 for $Agrp\text{-}Ucp2^{Tg}$, $p < 0.05$).

(F) Representative micro-CT images of femoral trabecular bone from 3-month-old male $Ucp2^{-/-}$ and $Ucp2^{-/-}$:*AgRP-Ucp2 Tg* mice. Scale bar, 500 μm.

(G and H) Micro-CT analysis revealed that the reduction in trabecular BV/TV and trabecular thickness seen in 3-month-old male $Ucp2^{-/-}$ mice is reversed by reactivating *Ucp2* in AgRP-expressing neurons ($Ucp2^{-/-}$:$Agrp\text{-}Ucp2^{Tg}$) (G: n = 3 for CT, n = 3 for $Ucp2^{-/-}$, n = 4 for $Ucp2^{-/-}$:$Agrp\text{-}Ucp2^{Tg}$; $p < 0.05$ for CT versus $Ucp2^{-/-}$, $p < 0.05$ for $Ucp2^{-/-}$ versus $Ucp2^{-/-}$:$Agrp\text{-}Ucp2^{Tg}$; H: n = 3 for CT, n = 3 for $Ucp2^{-/-}$, n = 4 for $Ucp2^{-/-}$:$Agrp\text{-}Ucp2^{Tg}$; $p < 0.05$ for CT versus $Ucp2^{-/-}$, $p = 0.0523$ for $Ucp2^{-/-}$ versus $Ucp2^{-/-}$:$Agrp\text{-}Ucp2^{Tg}$). *$p < 0.05$ and ***$p < 0.001$. Data are presented as means ± SEM. p values for unpaired comparisons were analyzed by Student's t test.

with AgRP-specific expression of Ucp2. These observations indicate that AgRP neurons are involved in bone metabolism and that the effect of Ucp2 on bone metabolism is mediated, at least in part by these hypothalamic neurons.

Neonatal Ablation of AgRP Neurons Results in Reduced Bone Mass

Next, we determined the skeletal phenotype of animals in which AgRP neurons are ablated perinatally using mice with AgRP neuron-specific diphtheria toxin receptors ($AgRP^{DTR}$). AgRP neurons can be experimentally ablated in these animals by diphtheria toxin injection (Luquet et al., 2005). While ablation of AgRP neurons in the adult results in rapid death due to aphagya, neonatal ablation of these cells is not lethal and does not result in altered feeding behavior (Luquet et al., 2005). We treated transgenic and control mice with diphtheria toxin at postnatal day 5 and analyzed the skeletal phenotype of adult animals. Micro-CT analysis showed that 3-month-old male $AgRP^{DTR}$ mice had significantly lower bone mass in both the trabecular and cortical compartments of the femora when compared with control mice (Figures 2A–2E). These data indicate that AgRP neurons are important for CNS-mediated modulation of bone metabolism during growth and development.

Impairment of AgRP Neuronal Excitability by Cell Autonomous Deletion of Sirt1 Results in Osteopenia

AgRP neurons in which the histone deacetylase, sirtuin 1 (Sirt1) was selectively deleted in vivo ($Agrp^{Sirt1-/-}$ mice) were neurobiologically active, but exhibited impaired excitation in response to metabolic cues, such as elevated ghrelin levels (Dietrich et al., 2010). We investigated the skeletal phenotype of $Agrp^{Sirt1-/-}$ mice. DXA scans demonstrated that 3-month-old male $Agrp^{Sirt1-/-}$ mice had reduced femoral BMD (Figure 3A). Micro-CT analysis revealed that there was a 30% decrease in trabecular bone volume in the femur (Figure 3C) accompanied by a reduction in trabecular thickness (Figure 3D), trabecular number, and connectivity density (data not shown) in 3-month-old male $Agrp^{Sirt1-/-}$ mice. Additionally, these mice displayed

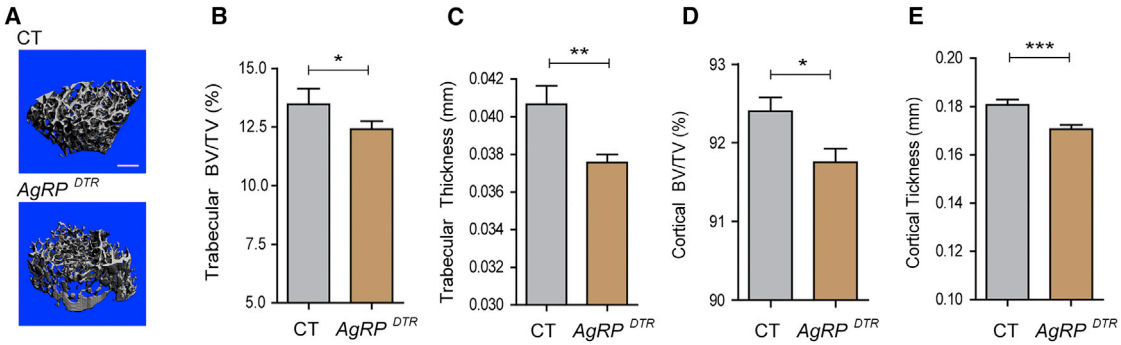

Figure 2. Early Postnatal Ablation of AgRP Neurons Results in Reduced Bone Mass

(A) Representative micro-CT images of femoral trabecular bone from 3-month-old male control (CT) and *AgRP*^{DTR} mice. Scale bar, 500 μm.

(B–E) Micro-CT analysis demonstrated a reduction in trabecular BV/TV, trabecular thickness, cortical BV/TV, and cortical thickness in 3-month-old male *AgRP*^{DTR} mice (B: n = 10 for CT, n = 20 for *AgRP*^{DTR}, $p < 0.05$; C: n = 10 for CT, n = 20 for *AgRP*^{DTR}, $p < 0.001$; D: n = 10 for CT, n = 20 for *AgRP*^{DTR}, $p < 0.05$; E: n = 10 for CT, n = 20 for *AgRP*^{DTR}, $p < 0.001$). *$p < 0.05$, **$p < 0.001$, and ***$p < 0.001$. Data are presented as means ± SEM. p values for unpaired comparisons were analyzed by Student's t test.

a significantly reduced cortical bone volume (Figure 3E) and thickness (Figure 3F). Consistent with the micro-CT findings, histomorphometric analysis of trabecular bone from 3-month-old male *Agrp*$^{Sirt1-/-}$ mice demonstrated a tendency toward reduced bone volume (Figure 3G) and trabecular thickness (Figure 3G). Histomorphometric analysis also indicated a trend toward reduced osteoblast numbers (Figure 3G) and an increase in osteoclast number (Figure 3G) albeit without statistical significance. However, entirely consistent with the trend toward an increase in osteoclast number, serum levels of carboxy-terminal collagen crosslinks (CTX), a marker of bone resorption, were significantly elevated in 3-month-old male *Agrp*$^{Sirt1-/-}$ mice (Figure 3H). These results suggest that a reduction in bone formation and an increase in bone resorption may contribute to the skeletal phenotype in AgRP circuit-impaired animals.

AgRP-Regulated Bone Metabolism Involves the Sympathetic Nervous System

The sympathetic nervous system (SNS) is an important mediator of CNS outputs to peripheral tissues. Multiple lines of evidence support a relationship between brain-regulated bone metabolism and centrally regulated peripheral sympathetic activity (Elefteriou et al., 2005; Yadav et al., 2009). Therefore, we analyzed whether sympathetic activity may be a mediator of AgRP neurons' effect on bone metabolism. Since *Ucp1* mediates β-adrenergic receptor-regulated thermogenesis in brown adipose tissue (BAT), we first tested *Ucp1* mRNA levels in BAT isolated from 3-month-old male *Ucp2*$^{-/-}$ mice, *Agrp-Ucp2*^{Tg} mice, and *Agrp*$^{Sirt1-/-}$ mice. We observed that *Ucp1* mRNA levels were significantly elevated in BAT isolated from osteopenic *Ucp2*$^{-/-}$ mice (Figure S2A) and *Agrp*$^{Sirt1-/-}$ mice (Figure 4A), whereas *Agrp-Ucp2*^{Tg} mice demonstrated a reduction in BAT *Ucp1* mRNA levels (Figure S2B). In addition, we found that the norepinephrine content in bone was higher in *Agrp*$^{Sirt1-/-}$ mice compared with controls (Figure 4B). To test whether elevated sympathetic outflow contributes to the osteopenia induced by impaired excitability of AgRP neurons, we evaluated bone mass in 3-month-old male control and *Agrp*$^{Sirt1-/-}$ mice treated with propranolol, a sympatholytic beta-blocker. Blockade of β-adrenergic receptors rendered BMD (Figure 4C) and trabecular bone mass (Figure 4D) indistinguishable in control and *Agrp*$^{Sirt1-/-}$ mice. These data indicate that attenuating the excitability of AgRP neurons results in increased sympathetic outflow, which in turn contributes to bone loss.

Leptin Receptors in AgRP Do Not Mediate Leptin's Action on Skeleton

The metabolic hormone, leptin, was shown to regulate bone metabolism by a central nervous system circuit (Ducy et al., 2000; Takeda et al., 2002). However, the exact cellular targets for leptin in the brain that mediate leptin's actions on the skeleton remain controversial. AgRP neurons are direct targets of leptin (Cowley et al., 2001; Heisler et al., 2006; Pinto et al., 2004). To test the role of leptin receptors in AgRP neurons in control of bone metabolism, we generated mice in which leptin receptors were cell-selectively ablated in AgRP neurons (*Agrp*$^{Lepr-/-}$ mice). 2-month-old male *Agrp*$^{Lepr-/-}$ mice displayed increased body weight and fat mass and lower lean mass (Figures S3A–S3C). However, BMD (Figure S3D) as well as trabecular and cortical BV/TV (Figures S3E and S3F) were not altered in these animals. These data indicate that leptin signaling in AgRP neurons is relevant to whole body energy metabolism, but appears to have less of an impact on bone homeostasis in healthy young mice. Whether leptin-regulated AgRP function plays a role in disease states, such as anorexia nervosa and lipodystrophy where hypoleptinemia is associated with impaired skeletal health (Misra and Klibanski, 2014; Moran et al., 2004), needs further investigation.

DISCUSSION

In this study we explored the involvement of AgRP neurons in the control of skeletal homeostasis. By using a variety of models, we observed that impaired AgRP circuit function leads to an osteopenic phenotype. The effect of AgRP neurons on bone metabolism in the adult is likely mediated, at least in part, by the

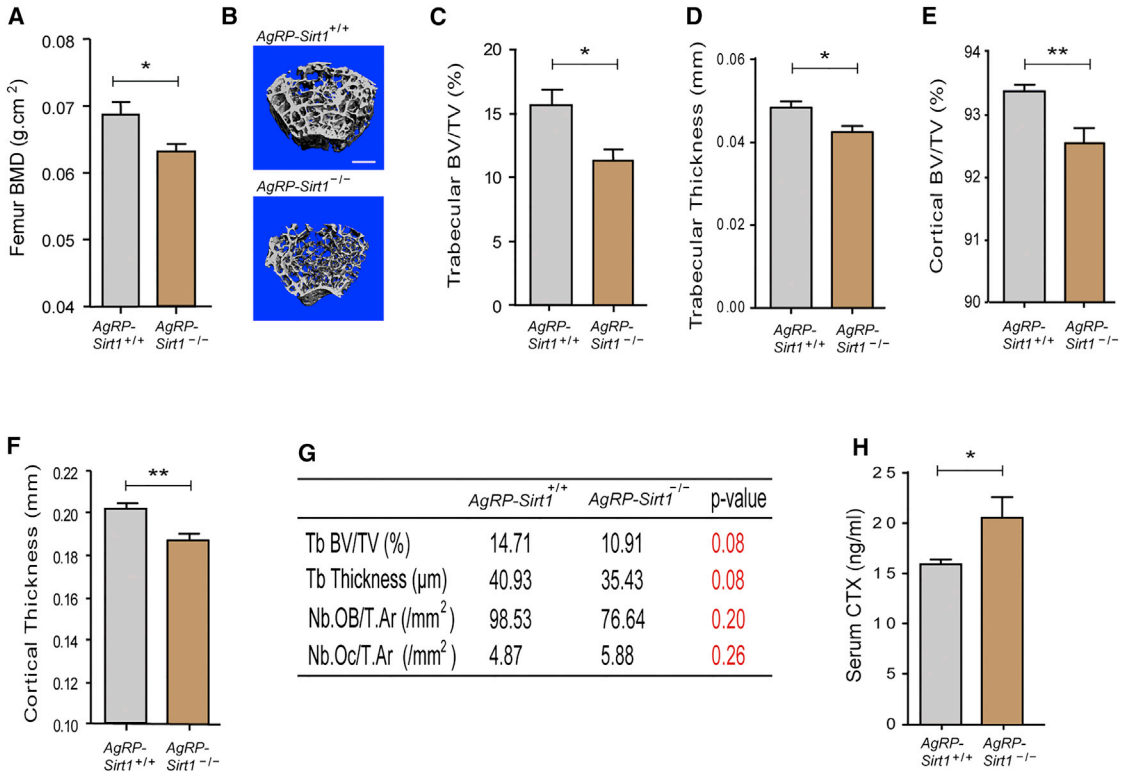

	AgRP-Sirt1$^{+/+}$	AgRP-Sirt1$^{-/-}$	p-value
Tb BV/TV (%)	14.71	10.91	0.08
Tb Thickness (μm)	40.93	35.43	0.08
Nb.OB/T.Ar (/mm^2)	98.53	76.64	0.20
Nb.Oc/T.Ar (/mm^2)	4.87	5.88	0.26

Figure 3. Impairing AgRP Neuronal Excitability by Deletion of *Sirt1* in AgRP Neurons Results in Reduced Bone Mass In Vivo

(A) DXA analysis demonstrated a reduced femoral bone density in 3-month-old male *Agrp*$^{Sirt1-/-}$ mice (n = 9 for *Agrp*$^{Sirt+/+}$, n = 9 for *Agrp*$^{Sirt1-/-}$, $p < 0.05$).

(B) Representative micro-CT images of femoral trabecular bone in 3-month-old male *Agrp*$^{Sirt\ +/+}$ and *Agrp*$^{Sirt1-/-}$ mice. Scale bar, 500 μm.

(C–F) Micro-CT analysis shows reduced trabecular BV/TV, trabecular thickness, cortical BV/TV and cortical thickness in 3-month-old male *Agrp*$^{Sirt1-/-}$ mice (C: n = 14 for *Agrp*$^{Sirt\ +/+}$, n = 12 for *Agrp*$^{Sirt1-/-}$, $p < 0.05$; D: n = 14 for *Agrp*$^{Sirt\ +/+}$, n = 12 for *Agrp*$^{Sirt1-/-}$, $p < 0.05$; E: n = 14 for *Agrp*$^{Sirt\ +/+}$, n = 12 for *Agrp*$^{Sirt1-/-}$, $p < 0.01$; F: n = 14 for *Agrp*$^{Sirt\ +/+}$, n = 12 for *Agrp*$^{Sirt1-/-}$, $p < 0.01$).

(G) Histomorphometric analysis of trabecular bone from 3-month-old male *Agrp*$^{Sirt1-/-}$ mice showed a trend toward a reduction in bone volume with lower numbers of osteoblasts and higher numbers of osteoclasts (n = 5 for *Agrp*$^{Sirt\ +/+}$, n = 5 for *Agrp*$^{Sirt1-/-}$).

(H) Serum levels of CTX were elevated in 3-month-old male *Agrp*$^{Sirt1-/-}$ mice (n = 6 for *Agrp*$^{Sirt\ +/+}$, n = 7 for *Agrp*$^{Sirt1-/-}$, $p < 0.05$). *$p < 0.05$ and **$p < 0.01$. Data are presented as means ± SEM. p values for unpaired comparisons were analyzed by Student's t test.

sympathetic nervous system, because suppression of beta adrenergic system abolished phenotype differences between *AgRP*$^{Sirt1-/-}$ and control mice. We found that global *Ucp2*-deficient mice displayed a significant reduction of bone mass accompanied by a reduction in bone formation without a change in bone resorprion. Selective re-expression of UCP2 in AgRP neurons in *Ucp2*$^{-/-}$ animals reversed the osteopenic phenotype, suggesting that AgRP neurons may be an important site where UCP2 exerts its effect on bone. However, *Ucp2* is widely expressed, and it is not unlikely that the skeletal phenotype of *Ucp2*$^{-/-}$ mice is due to multiple mechanisms. In line with this notion, histomorphometric analyses in *Agrp*$^{Sirt1-/-}$ mice revealed a trend toward reduced osteoblast number and an increase in osteoclast number, changes that were not observed in *Ucp2*$^{-/-}$ mice. This difference in the cellular changes in bone observed in *Ucp*$^{-/-}$ mice and *Agrp*$^{Sirt1-/-}$ mice could reflect a cell autonomous effect of global *Ucp2* deletion in bone cells.

Although more than one pathway likely mediates AgRP neuron-controlled bone mass, we did find evidence for an effector role of the sympathetic nervous system in the skeletal phenotype of the *AgRP*$^{Sirt1-/-}$ animals. We also found that a surrogate marker of sympathetic activation (brown fat UCP1 mRNA levels) was elevated in mice with AgRP circuit impairment and downregulated in mice with AgRP circuit enhancement. There are many other mechanisms by which the AgRP system can affect bone mass, including actions on the thyroid, adrenal, and gonadal axes. Further studies are needed to assess humoral control of bone metabolism modulated by AgRP neurons. Nonetheless, because at least in adult mice interference with the sympathetic tone reversed the bone phenotype of *AgRP*$^{Sirt1-/-}$ mice, it is reasonable to conclude that AgRP neuronal function in adult mice controls bone mass. Finally, since the models we employed alter AgRP function during development, it may be that changing AgRP signaling during skeletogenesis and modeling also contributed to the adult bone phenotype of the engineered lines that we studied.

Bone metabolism is tightly connected to nutrient availability. However, the genetic models we employed did not display significant differences in metabolic phenotypes or body length at

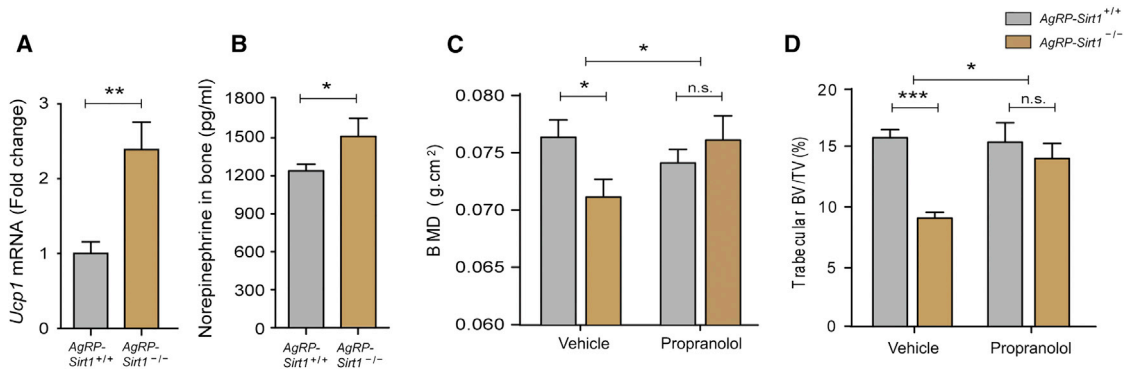

Figure 4. Osteopenia Seen in *Agrp*$^{Sirt1-/-}$ Mice Is Rescued by β-Adrenergic Blockade

(A and B) 3-month-old male *Agrp*$^{Sirt1-/-}$ mice had increased *Ucp1* transcript expression in brown adipose tissue and norepinephrine content in bone (A: n = 6 for *Agrp*$^{Sirt+/+}$, n = 8 for *Agrp*$^{Sirt1-/-}$, $p < 0.01$; B: n = 5 for *Agrp*$^{Sirt+/+}$, n = 4 for *Agrp*$^{Sirt1-/-}$, $p < 0.05$).

(C) DXA analysis demonstrated that the reduced femoral BMD seen in 3-month-old male *Agrp*$^{Sirt1-/-}$ mice was reversed by treatment with propranolol (n = 3 for *Agrp*$^{Sirt+/+}$ + vehicle, n = 4 for *Agrp*$^{Sirt1-/-}$ + vehicle, n = 3 for *Agrp*$^{Sirt+/+}$ + propranolol, n = 4 for *Agrp*$^{Sirt1-/-}$ + propranolol; $p < 0.05$ for Student's t test and two-way ANOVA).

(D) Micro-CT analysis demonstrated that the reduction in femoral trabecular BV/TV of 3-month-old male *Agrp*$^{Sirt1-/-}$ mice was rescued by treatment with propranolol (n = 9 for *Agrp*$^{Sirt+/+}$ + vehicle, n = 9 for *Agrp*$^{Sirt1-/-}$ + vehicle, n = 7 for *Agrp*$^{Sirt+/+}$ + propranolol, n = 7 for *Agrp*$^{Sirt1-/-}$ + propranolol, $p < 0.001$ for Student's t test; $p < 0.05$ for two-way ANOVA). *$p < 0.05$, **$p < 0.01$, and ***$p < 0.001$. Data are presented as means ± SEM. p values for unpaired comparisons were analyzed by Student's t test. Two-way ANOVA was performed to detect significant interaction between genotype and treatment (propranolol).

the ages they were studied when fed normal murine chow (Andrews et al., 2010; Dietrich et al., 2010; Luquet et al., 2005). These observations suggest that alternation of AgRP neuronal activities affects bone homeostasis independent of metabolic shifts. In further support of this notion, deletion of leptin receptors from AgRP neurons did alter the metabolic phenotype of mice without affecting bone mass. However, leptin signaling (or the lack thereof) in AgRP neurons may be relevant to disease states associated with impaired bone metabolism, such as anorexia nervosa or lipodistrophy.

Collectively, our findings demonstrate that hypothalamic AgRP neuronal circuit integrity is a regulator of bone mass and that this effect is mediated, at least in part, by the sympathetic nervous system. These results provide novel insights into the central regulatory component of bone metabolism and offer new strategies to consider in addressing skeletal dysregulation in various disease conditions.

EXPERIMENTAL PROCEDURES

Animals

The following transgenic mice were used in this study: *Agrp*$^{Sirt1-/-}$ mice were generated as described previously (Dietrich et al., 2010). *Agrp*^{DTR} mice were provided by Dr. R.D. Palmiter (University of Washington) and have been described previously (Luquet et al., 2005). *Ucp2*$^{-/-}$ mice were provided by Dr. B.B. Lowell (Harvard University) and have been used previously (Andrews et al., 2008). *Agrp-Ucp2*^{Tg} mice overexpressing *Ucp2* in AgRP neurons were generated by cre-lox knock in technology as described in Figure S1. In brief, a transgene (lower panel of Figure S1A) was engineered in which expression of the murine cDNA for Ucp2 is controlled by a CMV promoter when a transcriptional stop cassette is removed by cre recombination. (The Ucp2 cDNA was introduced into the construct using the Asc I restriction enzyme.) This transgene was then used to generate transgenic mice (*Ucp2*^{Tg} mice). To generate AgRP neuron-specific overexpression of the *Ucp2* gene, *Ucp2*^{Tg} mice were crossed with *AgRP-Ires*-cre mice (*Agrp*$^{tm1(cre)Lowl}$, Jax #012899). We controlled for ectopic expression of Cre in this AgRP line as described earlier (Dietrich et al., 2010, 2012), and those with ectopic expression were excluded from further studies. To generate AgRP neuron-specific *Ucp2*-reactivated *Ucp2*$^{-/-}$ mice (*Ucp2*$^{-/-}$*:Agrp-Ucp2*^{Tg} mice), *Ucp2*$^{-/-}$ mice were mated with *Agrp-Ucp2*^{Tg} mice. To generate a mouse line in which leptin receptor signaling in AgRP neurons is impaired, *AgRP-Ires*-cre mice were mated with *Lepr*$^{flox/flox}$ mice (McMinn et al., 2005) (generated by Streamson Chua, Albert Einstein College of Medicine) and breeding cages maintained by mating *Lepr*$^{flox/flox}$ and *Lepr*$^{flox/flox}$:AgRP Cre mice. *Agrp*^{DTR} or wild-type mice from the same litter received an injection of diphtheria toxin at postnatal day 5 (Luquet et al., 2005). All animals were kept in temperature- and humidity-controlled rooms on a 12-hr:12-hr light:dark cycle, with lights on from 7:00 a.m. to 7:00 p.m. Mice were group housed (three to five mice per cage), and food and water were provided ad libitum. All procedures were approved by the Institutional Animal Care and Use Committee of Yale University.

Histomorphometric Analyses

Static histomorphometry was performed as previously reported (Knopp et al., 2005). Analyses were performed on 5-μM thick sections of distal femur stained with toluidine blue (pH 3.7) using a Nikon microscope interfaced with the Osteomeasure system software and hardware (Osteometrics). Measurements were obtained in an area of cancellous bone that measures approximately 2.5 mm^2, containing only secondary spongiosa, and located 0.5–2.5 mm proximal to the epiphyseal growth cartilage. Longitudinal sections (5-μm thick) taken in the frontal plane through the cancellous bone of the femora are prepared with a Leica RM2165 microtome, mounted on chromalum coated glass slides, and stained with toluidine blue (pH 3.7). All indices are defined according to the American Society of Bone and Mineral Research histomorphometry nomenclature. We analyzed trabecular bone volume, trabecular thickness, the number of osteoblasts, and osteoclasts per trabecular area in 3-month-old male *Ucp2*$^{-/-}$ or *Agrp*$^{Sirt1-/-}$ mice compared with littermate control mice.

Bone Densitometry and Ultrastructural Analyses

Dual-energy X-ray absorptiometry (PIXImus) was used to determine fat mass, lean mass, and bone mineral density of 2- or 3-month-old male *Ucp2*$^{-/-}$, *Agrp-Ucp2*^{Tg}, *Agrp*$^{Sirt1-/-}$, and *Agrp*$^{Lepr-/-}$ mice. μCT (Scanco microCT35 machine) was used to separately assess the cortical and trabecular skeletal envelopes as well as microarchitectural features such as trabecular thickness for 2- or 3-month-old male *Ucp2*$^{-/-}$, *Agrp-Ucp2*^{Tg}, *Ucp2*$^{-/-}$*:Agrp-Ucp2*^{Tg}, *AgRP*^{DTR},

Agrp$^{Sirt1-/-}$, and *Agrp*$^{Lepr-/-}$ mice. All experiments were performed in the Yale Core Center for Musculoskeletal Disorders.

Propranolol Treatment

Propranolol (Sigma) was administered at a concentration of 0.5 mg/ml in the drinking water of *Agrp*$^{Sirt1-/-}$ and control mice for 4 weeks, from 10 weeks of age. Propranolol-containing water was refreshed three times per week. Control mice had normal drinking water. Mice were scanned by PIXImus to determine bone mineral density and sacrificed at the end of treatment followed by harvesting femora for micro-CT analysis.

Real-Time PCR

RNA from brown adipose tissue was isolated with the RNeasy Micro Kit (QIAGEN) and reverse transcribed to cDNA using MultiScribe Reverse Transcriptase (Applied Biosystems). Quantitative PCR was performed with the Light Cycler 480 Real-Time PCR system (Roche) using TaqMan probe (*Ucp1* [Mm01244861_m1], Applied Biosystems). The data were normalized with Glyceraldehyde-3-phosphate dehydrogenase (Gapdh [Mm99999915_g1], Applied Biosystems).

Measurement of Norepinephrine in Bone

Soft tissue was rapidly removed from the femur and tibia, and both bones were snap frozen in liquid nitrogen. The bone was then pulverized in 10 ml of freshly prepared 0.4 N perchloric acid containing 5 nM reduced glutathione and then centrifuged for 15 min at 1,300 × *g* to produce a protein-free supernatant. The entire supernatant was then adjusted to pH 7 and extracted on alumina columns. Catecholamines were analyzed in the extract by high-performance liquid chromatography using electrochemical detection (ESA Laboratories).

Measurement of Serum CTX

Serum CTX was measured using the RatLaps ELISA kit (Nordic Bioscience Diagnostics A/S).

Statistical Analyses

Statistical analyses were performed by use of Prism 6.0 software (Graph Pad). Data distribution was assumed to be normal, but this was not formally tested. No statistical methods were used to predetermine sample sizes, but our sample sizes are similar to those reported previously (Dietrich et al., 2012). All analyses were performed in a blinded manner. No randomization was used to assign experimental groups or to collect data, but mice were assigned to specific experimental groups without bias. An unpaired t test was performed to analyze the significance between the two experimental groups. Two-way ANOVA analysis was performed to detect the interaction between treatment and genotype. Significance was taken at $p < 0.05$.

SUPPLEMENTAL INFORMATION

Supplemental Information includes three figures and can be found with this article online at http://dx.doi.org/10.1016/j.celrep.2015.08.070.

AUTHOR CONTRIBUTIONS

J.G.K., M.O.D., K.I., and T.L.H. designed the study. J.G.K., K.I., and T.L.H. interpreted the results. J.G.K., M.K., G.-Q.Y., and B.-H.S. performed experiments and analyzed the data. J.G.K. contributed to all figures. B.-H.S. contributed to Figures 1,2, 3, and 4. G.-Q.Y. contributed to Figure 1D and Figure 3G. M.K. contributed to Figures 1F–1H and Figures 3B–3F. J.G.K., M.O.D., and S.D. contributed to the generation of animal model. J.G.K., K.I., and T.L.H. wrote the paper with input from the other authors.

ACKNOWLEDGMENTS

This work was supported by NIH grants R01 AG040236, DP1 DK098058, R01 DK097566, and P30 Core Center award AR46032, and an ADA Mentored Fellowship Award.

Received: March 9, 2015
Revised: July 9, 2015
Accepted: August 26, 2015
Published: September 24, 2015

REFERENCES

Andrews, Z.B., Liu, Z.W., Walllingford, N., Erion, D.M., Borok, E., Friedman, J.M., Tschöp, M.H., Shanabrough, M., Cline, G., Shulman, G.I., et al. (2008). UCP2 mediates ghrelin's action on NPY/AgRP neurons by lowering free radicals. Nature *454*, 846–851.

Andrews, Z.B., Erion, D.M., Beiler, R., Choi, C.S., Shulman, G.I., and Horvath, T.L. (2010). Uncoupling protein-2 decreases the lipogenic actions of ghrelin. Endocrinology *151*, 2078–2086.

Coppola, A., Liu, Z.W., Andrews, Z.B., Paradis, E., Roy, M.C., Friedman, J.M., Ricquier, D., Richard, D., Horvath, T.L., Gao, X.B., and Diano, S. (2007). A central thermogenic-like mechanism in feeding regulation: an interplay between arcuate nucleus T3 and UCP2. Cell Metab. *5*, 21–33.

Cowley, M.A., Smart, J.L., Rubinstein, M., Cerdán, M.G., Diano, S., Horvath, T.L., Cone, R.D., and Low, M.J. (2001). Leptin activates anorexigenic POMC neurons through a neural network in the arcuate nucleus. Nature *411*, 480–484.

Diano, S., and Horvath, T.L. (2012). Mitochondrial uncoupling protein 2 (UCP2) in glucose and lipid metabolism. Trends Mol. Med. *18*, 52–58.

Dietrich, M.O., Antunes, C., Geliang, G., Liu, Z.W., Borok, E., Nie, Y., Xu, A.W., Souza, D.O., Gao, Q., Diano, S., et al. (2010). Agrp neurons mediate Sirt1's action on the melanocortin system and energy balance: roles for Sirt1 in neuronal firing and synaptic plasticity. J. Neurosci. *30*, 11815–11825.

Dietrich, M.O., Bober, J., Ferreira, J.G., Tellez, L.A., Mineur, Y.S., Souza, D.O., Gao, X.B., Picciotto, M.R., Araújo, I., Liu, Z.W., and Horvath, T.L. (2012). AgRP neurons regulate development of dopamine neuronal plasticity and nonfood-associated behaviors. Nat. Neurosci. *15*, 1108–1110.

Ducy, P., Amling, M., Takeda, S., Priemel, M., Schilling, A.F., Beil, F.T., Shen, J., Vinson, C., Rueger, J.M., and Karsenty, G. (2000). Leptin inhibits bone formation through a hypothalamic relay: a central control of bone mass. Cell *100*, 197–207.

Elefteriou, F., Ahn, J.D., Takeda, S., Starbuck, M., Yang, X., Liu, X., Kondo, H., Richards, W.G., Bannon, T.W., Noda, M., et al. (2005). Leptin regulation of bone resorption by the sympathetic nervous system and CART. Nature *434*, 514–520.

Heisler, L.K., Jobst, E.E., Sutton, G.M., Zhou, L., Borok, E., Thornton-Jones, Z., Liu, H.Y., Zigman, J.M., Balthasar, N., Kishi, T., et al. (2006). Serotonin reciprocally regulates melanocortin neurons to modulate food intake. Neuron *51*, 239–249.

Horvath, T.L., Warden, C.H., Hajos, M., Lombardi, A., Goglia, F., and Diano, S. (1999). Brain uncoupling protein 2: uncoupled neuronal mitochondria predict thermal synapses in homeostatic centers. J. Neurosci. *19*, 10417–10427.

Joly-Amado, A., Denis, R.G., Castel, J., Lacombe, A., Cansell, C., Rouch, C., Kassis, N., Dairou, J., Cani, P.D., Ventura-Clapier, R., et al. (2012). Hypothalamic AgRP-neurons control peripheral substrate utilization and nutrient partitioning. EMBO J. *31*, 4276–4288.

Knopp, E., Troiano, N., Bouxsein, M., Sun, B.H., Lostritto, K., Gundberg, C., Dziura, J., and Insogna, K. (2005). The effect of aging on the skeletal response to intermittent treatment with parathyroid hormone. Endocrinology *146*, 1983–1990.

Luquet, S., Perez, F.A., Hnasko, T.S., and Palmiter, R.D. (2005). NPY/AgRP neurons are essential for feeding in adult mice but can be ablated in neonates. Science *310*, 683–685.

Matarese, G., Procaccini, C., Menale, C., Kim, J.G., Kim, J.D., Diano, S., Diano, N., De Rosa, V., Dietrich, M.O., and Horvath, T.L. (2013). Hunger-promoting hypothalamic neurons modulate effector and regulatory T-cell responses. Proc. Natl. Acad. Sci. USA *110*, 6193–6198.

McMinn, J.E., Liu, S.M., Liu, H., Dragatsis, I., Dietrich, P., Ludwig, T., Boozer, C.N., and Chua, S.C., Jr. (2005). Neuronal deletion of Lepr elicits diabesity in

mice without affecting cold tolerance or fertility. Am. J. Physiol. Endocrinol. Metab. *289*, E403–E411.

Misra, M., and Klibanski, A. (2014). Anorexia nervosa and bone. J. Endocrinol. *221*, R163–R176.

Moran, S.A., Patten, N., Young, J.R., Cochran, E., Sebring, N., Reynolds, J., Premkumar, A., Depaoli, A.M., Skarulis, M.C., Oral, E.A., and Gorden, P. (2004). Changes in body composition in patients with severe lipodystrophy after leptin replacement therapy. Metabolism *53*, 513–519.

Ohlsson, C., Engdahl, C., Börjesson, A.E., Windahl, S.H., Studer, E., Westberg, L., Eriksson, E., Koskela, A., Tuukkanen, J., Krust, A., et al. (2012). Estrogen receptor-α expression in neuronal cells affects bone mass. Proc. Natl. Acad. Sci. USA *109*, 983–988.

Pinto, S., Roseberry, A.G., Liu, H., Diano, S., Shanabrough, M., Cai, X., Friedman, J.M., and Horvath, T.L. (2004). Rapid rewiring of arcuate nucleus feeding circuits by leptin. Science *304*, 110–115.

Ruan, H.B., Dietrich, M.O., Liu, Z.W., Zimmer, M.R., Li, M.D., Singh, J.P., Zhang, K., Yin, R., Wu, J., Horvath, T.L., and Yang, X. (2014). O-GlcNAc transferase enables AgRP neurons to suppress browning of white fat. Cell *159*, 306–317.

Sato, S., Hanada, R., Kimura, A., Abe, T., Matsumoto, T., Iwasaki, M., Inose, H., Ida, T., Mieda, M., Takeuchi, Y., et al. (2007). Central control of bone remodeling by neuromedin U. Nat. Med. *13*, 1234–1240.

Takeda, S., Elefteriou, F., Levasseur, R., Liu, X., Zhao, L., Parker, K.L., Armstrong, D., Ducy, P., and Karsenty, G. (2002). Leptin regulates bone formation via the sympathetic nervous system. Cell *111*, 305–317.

Warne, J.P., Varonin, J.M., Nielsen, S.S., Olofsson, L.E., Kaelin, C.B., Chua, S., Jr., Barsh, G.S., Koliwad, S.K., and Xu, A.W. (2013). Retraction. J. Neurosci. *34* (*41*), 13865.

Yadav, V.K., Oury, F., Suda, N., Liu, Z.W., Gao, X.B., Confavreux, C., Klemenhagen, K.C., Tanaka, K.F., Gingrich, J.A., Guo, X.E., et al. (2009). A serotonin-dependent mechanism explains the leptin regulation of bone mass, appetite, and energy expenditure. Cell *138*, 976–989.